

Article

The Sticking of N₂ on W(100) Surface: An Improvement in the Description of the Adsorption Dynamics Further Reconciling Theory and Experiment

Maria Rutigliano ^{1,*}  and Fernando Pirani ^{2,3} 

¹ Istituto per la Scienza e Tecnologia dei Plasmi (ISTP), Consiglio Nazionale delle Ricerche (CNR), Via Amendola 122/D, 70126 Bari, Italy

² Dipartimento di Chimica, Biologia e Biotecnologie, Università di Perugia, Via Elce di Sotto 8, 06123 Perugia, Italy; pirani.fernando@gmail.com

³ Dipartimento di Ingegneria Civile ed Ambientale, Università di Perugia, Via G. Duranti 93, 06125 Perugia, Italy

* Correspondence: maria.rutigliano@cnr.it

Abstract: The adsorption of nitrogen molecules on a (100) tungsten surface has been studied using a new potential energy surface in which long-range interactions are suitably characterized and represented by the Improved Lennard–Jones function. The new potential energy surface is used to carry out molecular dynamics simulations by adopting a semiclassical collisional method that explicitly includes the interaction with the surface phonons. The results of the sticking probability, evaluated as a function of the collision energy, are in good agreement with those obtained in the experiments and improve the already good comparison recently obtained with calculations performed using interactions from the Density Functional Theory method and corrected for long-range van der Waals contributions. The dependence of trapping probability on the surface temperature for a well-defined collision energy has also been investigated.

Keywords: long-range interactions; molecular dynamics; sticking; tungsten; surface temperature effect



Citation: Rutigliano, M.; Pirani, F. The Sticking of N₂ on W(100) Surface: An Improvement in the Description of the Adsorption Dynamics Further Reconciling Theory and Experiment. *Molecules* **2023**, *28*, 7546. <https://doi.org/10.3390/molecules28227546>

Academic Editor: Enrico Bodo

Received: 10 October 2023

Revised: 7 November 2023

Accepted: 10 November 2023

Published: 11 November 2023



Copyright: © 2023 by the authors. Licensee MDPI, Basel, Switzerland. This article is an open access article distributed under the terms and conditions of the Creative Commons Attribution (CC BY) license (<https://creativecommons.org/licenses/by/4.0/>).

1. Introduction

The adsorption of gaseous species on surfaces is of fundamental interest for many processes useful in different applied fields (see, for instance, Refs. [1,2] and the references therein). For this reason, over the years, the complexity of interacting species and the considered substrate has increased.

The reliability of the dynamics and kinetics of the adsorption process, evaluated by computational methods, relies on the accuracy of the used potential energy surface (PES) controlling the evolution of single collision events. In this regard, over the years, with the concomitant advent of powerful supercomputers, it has been possible to determine the PES using increasingly precise and refined methods [3]. The determination of the interaction driving the collisions in heterogeneous gas–surface systems poses different problems, from both the theoretical and computational points of view, primarily for the fact that the involved PES is multidimensional, being dependent on six coordinates. As a consequence, and also due to the large computational time demanded to assure the convergence of calculated energies, complete, fully dimensional electronic structure calculations have been performed for a few elementary systems, notably those involving diatomic molecules on noble and transition metals [4,5]. Among the proposed approximate schemes, the most promising approach is the Density Functional Theory (DFT), which is accurate near the chemisorption potential well, but less accurate for weak long-range interactions. Such weak components are of non-covalent nature and control the gas–surface trapping (physisorption). Therefore, they promote the formation of the precursor (or pre-reactive) state

of basic elementary processes, whose role in molecular dynamics is not trivial to identify. In this paper, we have addressed and tried to solve this last point for N₂ adsorption on a W(100) surface.

In the last decade, several studies have appeared in the literature [6–8] with an aim to explain the steep decrease in the sticking probability, the collision energy increasing up to 0.5 eV, as obtained in the experiments made in the late eighties [9–11] for nitrogen molecules impinging a W(100) surface. These experiments, in the same collision energy range, also revealed a different reactivity to the case in which nitrogen molecules impact W(110) [12,13]. Understanding and rationalizing the nitrogen adsorption process on tungsten can help to understand and explain the processes that occur on other metal surfaces of interest in nitrogen industrial processes, the ammonia synthesis in primis, which usually involves the interaction of N₂ and H₂, mainly with an iron surface [14].

The authors of Ref. [7] succeeded in significantly improving the previous results of simulations reported in Ref. [15] concerning the behavior of the sticking probability as a function of collision energy for N₂ on W(100), as obtained in experiments [9–11]. This improvement was obtained by adopting a PES determined by DFT calculations, including long-range interactions via the vdW-DF2 functional as implemented in the VASP code [16]. The authors of Ref. [7] ascribe the improvement in comparison with the experimental results to the fact that with the introduction of long-range interactions, the barrier in the entrance channel, revealed in the PES of Ref. [15], disappears.

The same authors investigated the energy dissipation during the adsorption dynamics of nitrogen molecules by the Generalized Langevin Oscillator (GLO) for molecule–surface interaction, whilst the Local Density Friction Approximation (LDFA) is implemented to consider the electron–hole (e–h) pair excitations [8]. From this study, it emerged that the interaction with the surface atoms plays a key role in the reaction energetics, while the e–h excitations rather influence the ratio between dissociative and non-dissociative adsorptions [8].

Recently, we proved that the Improved Lennard–Jones (ILJ) potential function [17] can also be useful and accurate for a proper description of the weak long-range non-covalent interactions between gaseous molecules and surfaces arising from the combination of size repulsion with dispersion attraction and controlling the physisorption state formation [18]. The accuracy of this description is derived from the fact that the adopted parameters relate to the intrinsic chemical–physical properties of the reaction partners. Moreover, by adopting the ILJ potential in conjunction with state-to-state molecular dynamics (MD) simulations based on a semiclassical collisional model [19,20], including the interaction with the surface phonons, treated in a quantum way, we were able to explain and support observations made in molecular beams (MB) experiments [21]. In addition, for each simplest-reference interacting pair, the ILJ function provides an asymptotic dispersion attraction associated with a C₆ coefficient, from which the atom/molecule–surface dispersion coefficient C₃ can also be evaluated (see next Sections 2 and 3).

Therefore, this work aims to apply our computational setup to the N₂-tungsten system to improve further the comparison between experiment and theory for the sticking probability and, at the same time, to provide an additional contribution to understanding reaction dynamics and the underlying energetics. To do this, we mainly focused on the evaluation of the long-range interaction strength, while also determining the C₆ and C₃ coefficients.

We built a new PES by grafting the short-range interaction data, taken from the literature, onto the long-range interaction modeled according to the ILJ potential. Then, we used the obtained PES, given in the proper analytical form, for MD simulations of N₂ molecules impinging the W(100) surface in the low-collision-energy range. The surface temperature (T_s) effect on the sticking probability, due to being related closely to the energy exchange with the phonons, explicitly considered in the adopted method, has also been investigated. The proper inclusion of surface phonons produces an agreement improved with the experimental results, whilst the correct treatment of the long-range interaction determining the precursor state suggests a new picture for the reaction dynamics.

Thus, the paper is organized in the following way: Section 2 focuses on the results obtained for the long-range interaction potential for the three active sites on the W(100) surface and provides the dispersion coefficients, which are also compared with the results available in the literature; in the same section, the results obtained for the sticking probability as a function of collision energy and surface temperature will be presented and discussed. Section 3 provides all basic details of the methods employed to carry out MD simulations and to formulate the PES. Some conclusions are drawn in Section 4.

2. Results and Discussion

2.1. The ILJ Long-Range Potential of N and N₂ Interacting with W(100)

Details on the ILJ formulation, representing the weak long-range non-covalent part of each interaction potential, are summarized in the Section 3. Table 1 provides values of the basic ILJ potential parameters and of related C₃ and C₆ dispersion coefficients. By exploiting high-resolution gas-phase MB experiments, it has been demonstrated [17] that the C₆ coefficients, representative of the asymptotic behavior of the ILJ potential, are in good agreement with the results obtained from other experimental sources, semiempirical predictions and/or ab initio calculations. In this section, the focus is on the asymptotic part of the PES affecting the gas–surface trapping and on the comparison between the C₃ coefficients, obtained in an internally consistent way from the ILJ C₆ coefficients, with the results available in the literature. In particular, the parameters reported in Table 1 have been evaluated, according to Refs. [17,22], by exploiting the polarizability of the single, isolated N atom (1.1 Å³) and the effective polarizability value of N in N₂ (0.88 Å³). We also estimated the value of the effective polarizability of each W atom bound in the surface equal to 2.9 Å³ and considered an atomic surface density (ρ) equal to 0.0632 atom/Å³. In Figure 1, the C₃ coefficient for the nitrogen atom and molecule is reported as a function of their polarizability (α) in comparison with the values, determined with the same method, for rare gases interacting with W(100). In the same figure, the C₃ coefficients for the interaction of rare gases with W(100), obtained with different methods [23], are reported for a useful comparison. Looking at the plot, we can infer both the linear correlation between the C₃ coefficient and α, and a good comparison between the data reported in the literature and those calculated in this work for rare gases. Moreover, the right placement of points for N and N₂ in the plot makes us confident about the parameters used to obtain the long-range potential of interest for the present investigation.

Table 1. ILJ adopted parameters and related dispersion coefficients. Note that ε, R_m and C₆ represent, respectively, the potential well, the minimum location and the dispersion attraction coefficient of each weak interacting effective atom–effective atom pair. β, related to the hardness of the partners, is a parameter defining the shape of the potential well. The C₃ coefficient, defining the long-range atom/molecule–surface dispersion attraction, is proportional to C₆ multiplied by the atomic surface density (for further details, see the Section 3).

Interaction	ε (meV)	R _m (Å)	β	C ₆ (meV Å ⁶)	C ₃ (meV Å ³)
N(N ₂)–W	6.23	4.07	6.3	28,452	941.5
N–W	7.40	4.07	7.0	33,635	1119

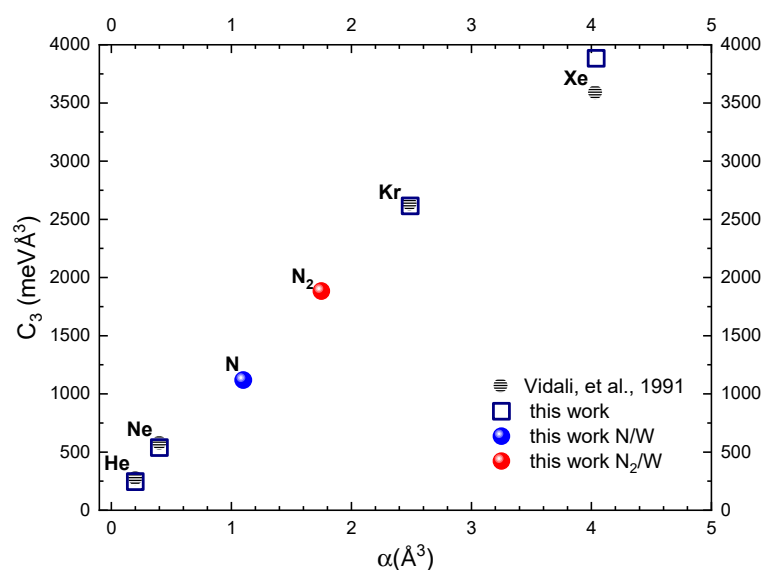


Figure 1. C_3 coefficients calculated for rare gases and nitrogen (atomic and molecular) as a function of polarizability (α) of the gaseous species interacting with W(100) in comparison with the data of Ref. [23]. The polarizability values of rare gas atoms and N_2 are taken from Ref. [24] and that of N from Ref. [25]. Note that while the relative C_3 values vary almost linearly with the rare gas atoms' polarizability, their absolute value also depends on the effective polarizability of W atoms bounded in the surface.

In Figure 2, the ILJ potential for the three active sites on the surface, top (T) on a W atom, bridge (B) between two adjacent W atoms and hollow (H) in the center of the bcc unit cell, are reported for N_2 impinging with the center of mass (CM) on the given site for two different orientations of the molecular axis with respect to the surface plane, parallel and perpendicular. In the same Figure, the ILJ potential for the N atom is also provided for the three sites.

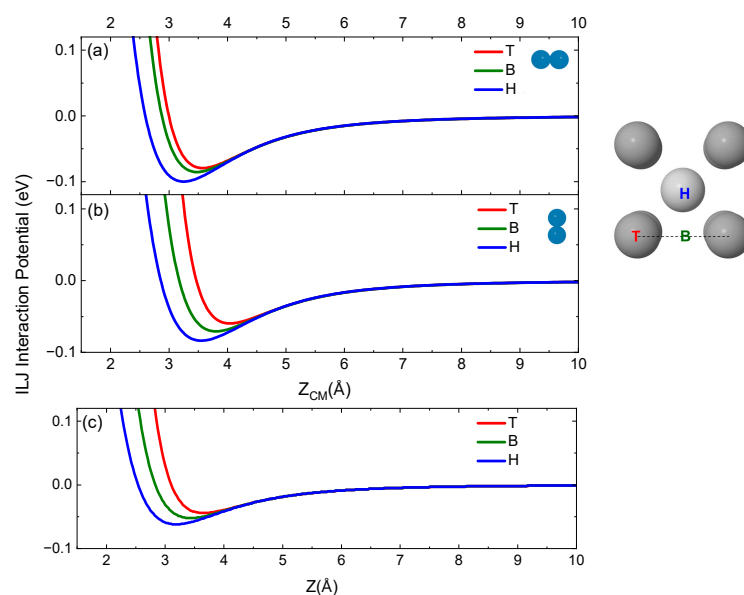


Figure 2. ILJ potential for N_2 impinging with its CM on T, B and H sites and with molecular axis being (a) parallel and (b) perpendicular to the surface plane. (c) ILJ potential for nitrogen atom impinging on the three sites. On the right side of the figure is the top view of the unit cell of W(100) on which the three sites on the surface are located. The color of the curves is associated with that of the site label. In the plot, Z defines the component of R along the normal direction and $Z = 0$ corresponds to the surface first layer.

From Figure 2, it emerges that the H site is the most attractive and that the minimum is placed at shorter distances from the surface compared with the other sites. Furthermore, for both atom and molecule, the physisorption well depth decreases with the sites according to the $H > B > T$ order. Moreover, for the same site, the molecule in parallel configuration undergoes greater attraction, with the well depth being close to 0.1 eV for the H site.

2.2. Potential Energy Surface Determination

The complete reactive PES has been obtained as a sum of pairwise interactions, according to the consolidated functional form already used for the study of several molecule–surface systems [21] and given in Equation (1).

$$V(\mathbf{r}, \mathbf{R}) = V_{\text{N}_2}(\mathbf{R}) \times \text{fsw}(\mathbf{r}) + V_{\text{N}}(\mathbf{R}) \times (1 - \text{fsw}(\mathbf{r})) \quad (1)$$

$V_{\text{N}_2}(\mathbf{R})$ and $V_{\text{N}}(\mathbf{R})$ represent (nitrogen molecule)– and (nitrogen atom)–surface interaction potentials, respectively. \mathbf{R} is the distance of impinging species from the surface. The weight function $\text{fsw}(\mathbf{r})$ switches the interaction potential between V_{N_2} and V_{N} as \mathbf{r} , the interatomic distance between the atoms in the molecule, increases and is given by

$$\text{fsw}(\mathbf{r}) = -0.5 \times ((\tanh(1.65 \times \mathbf{r} - 3.7)) - 1.0) \quad (2)$$

This function has been chosen to provide quick switching between 1 and 0, preserving the values of V_{N_2} and V_{N} for \mathbf{r} lower and higher, respectively, than the intramolecular distance considered critical for N_2 molecule dissociation ($3 \div 3.5 \text{ \AA}$).

$V_{\text{N}_2}(\mathbf{R})$ has been obtained by combining the interaction potential on the three different sites (see Figure 2) on the surface through a switch function fsw_{hbt} , given in Equation (4):

$$V_{\text{N}_2}(\mathbf{R}) = \sum_{j=1}^2 \sum_{i=1}^{\text{N}_{\text{at}}} [V_{\text{H}} \times \text{fsw}_{\text{hbt}} + (1 - \text{fsw}_{\text{hbt}}) \times (V_{\text{T}} \times (1 - \text{fsw}_{\text{bt}}) + V_{\text{B}} \times \text{fsw}_{\text{bt}})] \quad (3)$$

the sum on j runs on the two atoms in the molecule while that on i runs on the atoms N_{at} in the assumed surface model lattice.

$$\text{fsw}_{\text{hbt}} = (\text{FA})^2 \times \text{FB} \quad (4)$$

with

$$\text{FA} = \cos\left(1.5 \times \pi + \pi \times \frac{X_{\text{g}}}{a}\right) \text{ and } \text{FB} = \left|\sin\left(\pi \times \frac{Y_{\text{g}}}{a}\right)\right|$$

X_{g} and Y_{g} are the molecule CM coordinates on the X–Y plane of the assumed reference frame; a is the lattice constant of $\text{W}(100)$, equal to 3.165 \AA .

fsw_{bt} is another switching function to discriminate between B and T sites and has the following functional form:

$$\text{fsw}_{\text{bt}} = |\text{F1} + \text{F2}| \text{ with } \text{F1} = \sin\left(\pi \times \frac{X_{\text{g}}}{a}\right) \text{ and } \text{F2} = \sin\left(\pi \times \frac{Y_{\text{g}}}{a}\right) \quad (5)$$

The interaction potential for the H site is determined as a pure ILJ potential according to the data available in the literature [6,26] for both orientations of N_2 molecule impinging to the surface. Instead, for sites T and B, the ILJ potential was added to the fitting value of the potential determined in Refs. [6,26] for the incidence of N_2 in a perpendicular and parallel configuration, respectively. In fact, the authors of both papers determine the interaction potentials for distances up to $4.0 \div 5.0 \text{ \AA}$, too short to control the asymptotic behavior at longer distances, responsible for the formation of the precursor state.

For V_T and V_B , the expression, as a function of the CM distance along the normal to the surface of the incident molecule, is

$$V_S = \begin{cases} D_S \times e^{-b_S \times (R-R_S)} \times (e^{-b_S \times (R-R_S)} - 2) + x_S & Z_g < Z_S \\ V_{ILJ} & Z_g \geq Z_S \end{cases} \quad (6)$$

where Z_g is the Z coordinate of molecule CM in the assumed reference frame.

The subscript S from here can be T or B. Note that the switch between the two functional expressions of the potential occurs as a function of Z, the component along the normal direction to the X–Y plane of R.

The general expression for the parameter P (P generally indicating the D_S , b_S and R_S Morse function parameters; x_S being the additional long-range correction factor; and Z_S denoting the switch value for Z) depends on the site and orientation of the molecular axis (θ) relative to the surface plane. Then, its analytic form is $P = A + B(1 - \cos(\theta))$ and the values of the constants for each site are given in Table 2.

Table 2. Constant for the potential parameters for T and B sites for N_2 impacting on W(100).

Site	D_S (eV)		b_S (\AA^{-1})		R_S (\AA)		x_S (eV)		Z_S (\AA)	
	A	B	A	B	A	B	A	B	A	B
T	0.693	−0.675	1.16	3.59	2.54	−0.01	0.0079	−0.0079	2.95	0.07
B	0.390	−0.155	1.25	1.1	2.89	−0.63	0.0065	−0.0057	2.72	−0.03

The complete interaction potential for the N_2 molecule impinging with perpendicular and parallel orientation of its molecular axis and with CM on the three active sites on the W(100) surface is reported in Figure 3a,b.

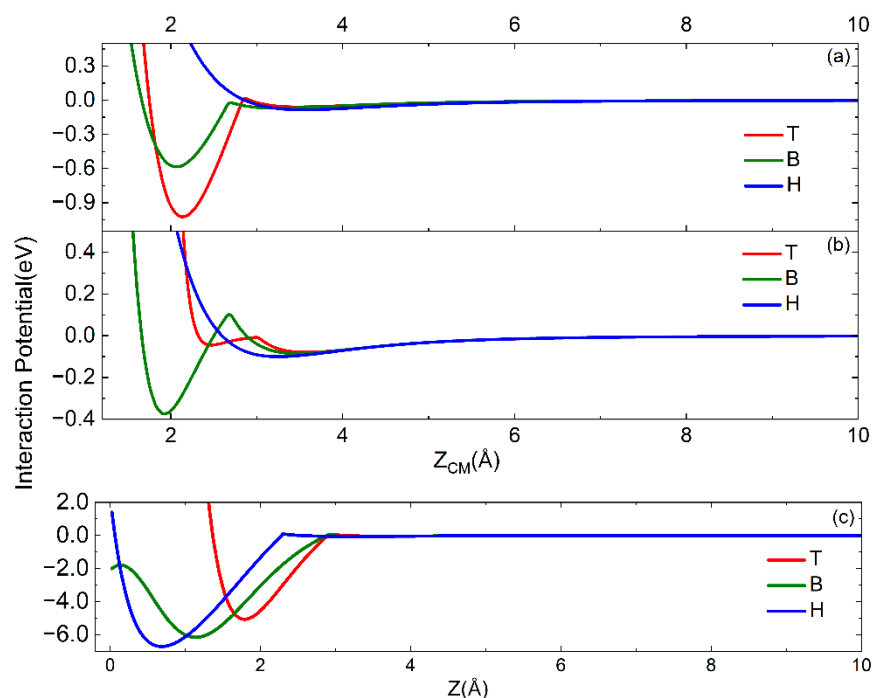


Figure 3. Interaction potentials for N_2 impinging with CM on T, B and H sites and with molecular axis (a) parallel and (b) perpendicular to the surface plane. (c) Interaction potential for nitrogen atom impinging on the three sites. The correspondence between the colors of the curves and the sites is the same as in Figure 2.

The interaction potential for atomic nitrogen for short distances has been obtained by fitting the results of Refs. [6,27]. The analytical form for V_N is the same as Equation (3).

For atomic nitrogen also, the interaction potential for the H site is obtained as the sum of short- and long-range contributions. The terms corresponding to the different sites are given similarly by the expression of Equation (6), while the corresponding parameters are reported in Table 3. The behavior of the obtained potential is reported in Figure 3c.

Table 3. Constants for the potential parameters of T, B and H sites for N impacting on W(100).

Site	D_S (eV)	b_S (\AA^{-1})	R_S (\AA)	x_S (eV)	Z_S (\AA)
T	3.845	1.45	1.97	0.014	2.88
B	2.35	1.75	2.08	0.0051	2.95
H	1.69	1.50	2.42	0.018	2.30

Looking at Figure 3, it is clear that the PES for the interaction of N and N_2 on W(100) results strongly corrugated. It is interesting to note that the molecular approach towards well-defined surface sites can introduce a small barrier for the transition from the physisorption well to the chemisorption well.

2.3. The Sticking Probability for N_2 Interacting on W(100)

The values of sticking probability as a function of N_2 collision energy (E_{coll}) obtained by MD simulations are reported in Figure 4 for $T_S = 300$ K in comparison with experimental data [10] and the results of previous simulations [7]. The values reported in the plot are obtained by including both dissociative and molecular adsorption events. Looking at the plot, it appears that the comparison with experimental results is improved significantly with respect to the comparison with the results of Ref. [7], mainly for the lower collision energies ($E_{\text{coll}} < 0.2$ eV). In particular, in this energy range, the slope with which the sticking probability (P_{Sticking}) decreases is almost the same as that of the experimental data. These findings, in comparison with those of Ref. [7], could indicate a different mechanism in the interaction dynamics due to the adoption of a dissimilar long-range interaction potential and/or that the treatment of the interaction with the phonons of the surface adopted here is able to describe better the energy exchanges between the incident species and the surface.

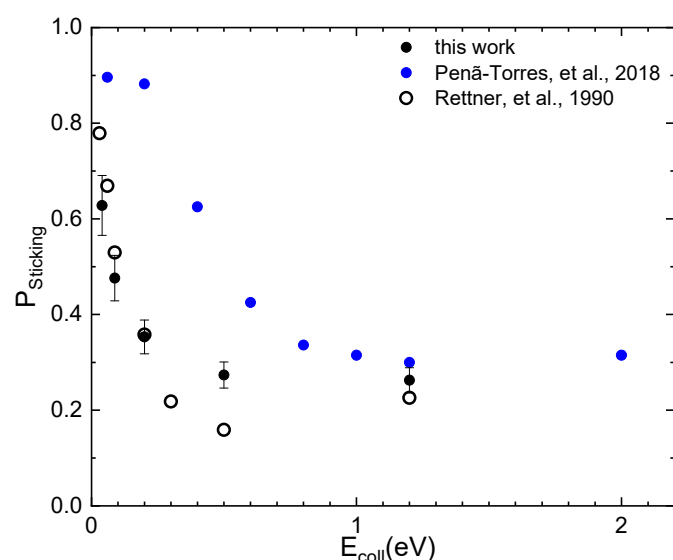


Figure 4. Sticking probability (P_{Sticking}) for N_2 interacting in normal direction on W(100) as a function of collision energy in comparison with results of latest calculations [7] and of experiments [10]. $T_S = 300$ K.

To settle the matter, an accurate analysis of the trajectories has been carried out to highlight the energy exchanges occurring between the internal degrees of the molecule and the surface. The analysis revealed that, for low collision energies and with the molecule

in the lowest internal state, the interaction is strong mainly when the molecules approach the surface by moving with a cartwheel-type internal motion. In this case, the rotational excitation mechanism, being the most efficient, favors the trapping that, in turn, can promote bounces on the surface, also contributing to the desynchronization of the motion of the two N atoms in the molecule. This behavior has already been observed in the interaction of nitrogen molecules with a graphite surface [21] and related to the surface phonons. In addition, as observed in previous studies for the interaction of molecules with graphite and silica surfaces [20,21,28], the molecule approaching the surface is first slightly accelerated and then undergoes a strong deceleration while transferring energy to the rotational motion. Consequently, a strong increment of the rotational number occurs to which the energy coming from the phonons of the surface also contributes, albeit with a smaller amount. The occurrence of such a trapping mechanism has already been advanced in Ref. [29] to explain the adsorption of hydrogen molecules on a cold Cu surface. Therefore, in light of the above, the obtained results for P_{Sticking} can be explained in terms of a dynamic steering mechanism. In our picture of interaction dynamics, the rotational excitation counteracts the steering that favors the molecule path towards a direct dissociation and molecules remain trapped on the surface. In the past, the role of rotational effect in the adsorption of molecules on metals has been observed in the MB experiments [30,31] and studied in Refs. [32,33]. In addition to the dynamic steering, the results for P_{Sticking} , for low collision energies, can also be ascribed to either the physisorption well appearing in the assumed PES and having a depth greater than or, at most, of the same order (see Section 2.2) as E_{coll} , which prevents the molecule from being immediately scattered in gas-phase, and/or to the existence of a barrier that can be higher than the collisional energy. The dynamic mechanism just described can be observed in Figure 5, which shows one of the trajectories ending with molecular adsorption for $E_{\text{coll}} = 0.04$ eV.

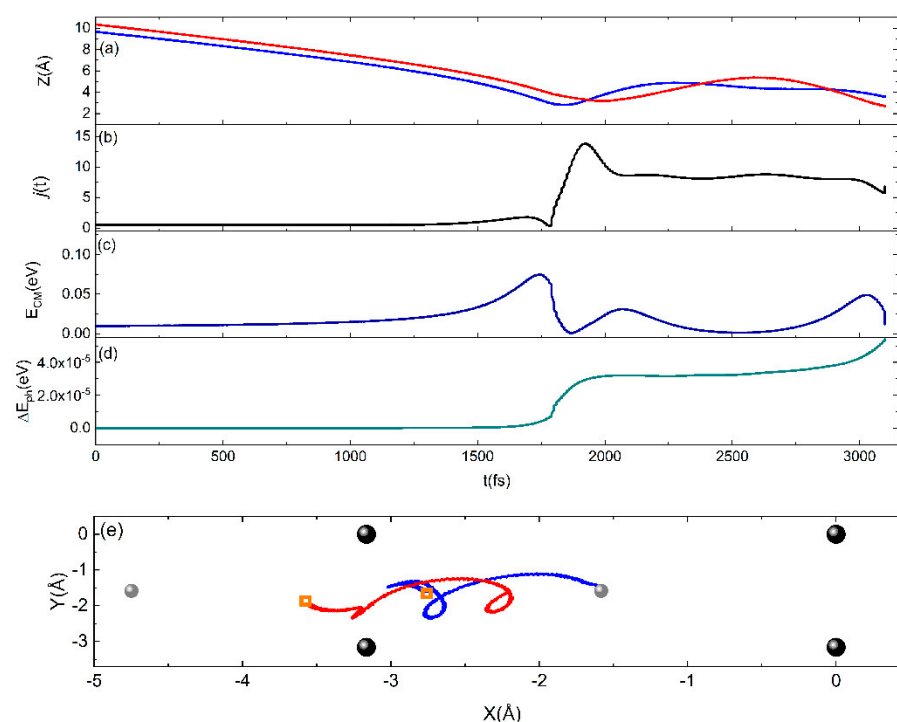


Figure 5. A typical sticking trajectory for $E_{\text{coll}} = 0.04$ eV. Time evolution of (a) the coordinate of the two atoms (lines blue and red) in the N_2 molecule, along the Z normal direction, which ends with the

adsorption; (b) the rotational state j ; (c) the center of mass translational energy (E_{CM}); (d) the energy exchanged with the surface phonons; and (e) the diffusion motion in the X – Y plane, of assumed reference frame, of the trajectory of two atoms (blue and red lines) in the N_2 molecule (orange squares indicate the starting point of each trajectory). The W atoms on the first (big black spheres) and second (small grey spheres) layers are also reported.

Thus, the ILJ potential used to treat the long-range interactions exploited by a state-to-state model, including the coupling with the surface phonon motion, is able to highlight molecular excitation governing the process dynamics and, with respect to previous calculations, provides results much closer to those resulting from experimental measurements.

The role of coupling of the N_2 molecule with phonons is further extolled by considering, at a selected collision energy, the dependence of the trapping probability ($P_{trapping}$) on T_S . $P_{trapping}$ represents the probability for a molecule to become trapped on the surface or eventually, after a while spent bouncing on the latter, to be scattered in the gas-phase. We did this, and in Figure 6, we report the results of our study in comparison with those reported in Ref. [10], obtained by adopting a hard cube model with parameters chosen to provide results consistent with experimental measurements. Looking at Figure 6, we can conclude that, even in this case, there is a very good agreement, considering the error of our results and the approximations and parametrization of Ref. [10] to obtain the line in the plot based on experimental measurements.

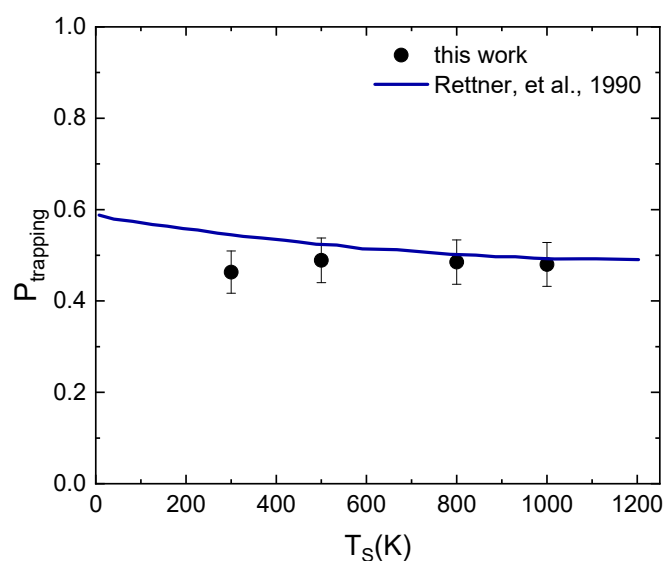


Figure 6. Trapping probability ($P_{trapping}$) for N_2 interacting on $W(100)$ as a function of surface temperature (T_S) at $E_{coll} = 0.088$ eV in comparison with results obtained in Ref. [10].

The plot in Figure 6 also suggests a weak dependence on the surface temperature of $P_{trapping}$, which appears to be more strongly correlated to the collision energy of the molecule and the energy exchanges occurring during the interaction. Such almost non-dependence on the surface temperature of $P_{trapping}$ can perhaps be attributed to the mass mismatch between the incident species and the substrate.

3. Methods

The computational setup, used to describe the collisions of atomic and molecular nitrogen with $W(100)$ surface, is based on a state-to-state semiclassical collision method, derived and completely exposed in Ref. [19], which has been used in the past for the description of surface processes; therefore, it has already been extensively described elsewhere [34] and more recently in Ref. [20]. For this reason, in the following, only a brief summary of the most important and specific features will be provided.

The method consists of three different operational steps: (1) determination of 3D surface model structure and corresponding surface phonon dynamics; (2) building up of PES for the reaction under study; and (3) propagation of a sufficiently large number of classical trajectories in the adopted framework [19,20].

The 3D surface model, consisting of 255 atoms disposed on six layers, is the one defined in Ref. [34] for which we determined the phonon dynamics by solving the time-dependent Schrödinger equations of motion under the harmonic oscillator approximation—that is, assuming that a set of $M = 3N_{\text{at}} - 6$ independent harmonic oscillators are perturbed by a linear force exerted between the species approaching the surface from the gas-phase and the solid substrate [19]. Details on the bulk potential and the density of phonon states can be found in Ref. [34].

The PES has been built by adding to the short-range potential (described in Section 2.2) the long-range interactions according to the ILJ potential [17] given by

$$V_{\text{ILJ}}(R) = \epsilon \left[\frac{m}{n(R) - m} \left(\frac{R_m}{R} \right)^{n(R)} - \frac{n(R)}{n(R) - m} \left(\frac{R_m}{R} \right)^m \right] \quad (7)$$

with

$$n(R) = \beta + 4 \left(\frac{R}{R_m} \right)^2 \quad (8)$$

The first term of Equation (7) describes the separation distance dependence of the size repulsion, while the second one is that of the dispersion attraction. The parameters ϵ and R_m , which represent the potential well depth and its location, respectively, for each considered pair, define at each R the strength of both terms in Equation (7). β is an additional parameter depending on the “hardness” of the two partners. For the neutral–neutral interactions, as in the present ones, $m = 6$ must be used: in these cases, the ILJ function provides for each interacting pair an asymptotic dispersion attraction contribution associated with a partial C_6 coefficient, defined as $C_6 = \epsilon \times R_m^6$. The combination of all partial C_6 coefficients determines the value of the global atom/molecule–surface attraction coefficient C_3 , which controls the capture efficiency and the formation of the precursor state of many gas–surface elementary processes. The C_3 coefficient is obtained through the well-known relationship (see Ref. [21] and references therein) that binds it to the C_6 coefficient:

$$C_3 = \frac{\pi \times C_6 \times \rho}{6} \quad (9)$$

The dynamics of the N_2 molecule interacting with W(100) surface is followed by solving self-consistently the relevant 3D Hamilton’s equations of motion with those of the lattice phonons, under given initial conditions:

$$\dot{R}_i = \frac{\partial H}{\partial P_i}; \quad \dot{P}_i = -\frac{\partial H}{\partial R_i} \quad (10)$$

P_i is the momentum of atom i having mass m_i and H is the Hamiltonian for a diatomic molecule impinging on a surface, given by

$$H = \frac{1}{2} \sum_i \frac{P_i^2}{m_i} + V_{N_2}(r) + \Delta E_{\text{ph}} + V_{\text{eff}}(t, T_S) \quad (11)$$

with $V_{N_2}(r)$ being the N_2 intramolecular interaction potential and $V_{\text{eff}}(t, T_S)$ the effective potential of mean field type, depending on time and surface temperature, formulated as

$$V_{\text{eff}}(t, T_S) = V_0 + \sum_k V_K^{(1)} \eta_k(t) \quad (12)$$

where V_0 is the “static” interaction potential, given by Equation (1), between the atoms in the gas-phase and the lattice atoms in their equilibrium positions. $V_k^{(1)} = \partial V(r, R) / \partial Q_k |_{\text{eq}}$

is the linear driving force exerted on each k -th phonon mode Q_k . η_k are the “phonon excitation strengths” given in terms of the Fourier components $I_{i,k}$ of the external force:

$$\eta_k(t) = - \int dt' (\hbar\omega_k)^{-1} \frac{d}{d\rho_k} (\Delta E_k^+ + \Delta E_k^-) [I_{c,k}(t') \cos(\Theta_k(t', \omega_k)) + I_{s,k}(t') \sin(\Theta_k(t', \omega_k))] \quad (13)$$

$$I_{c,k} = \int_{-\infty}^{+\infty} dt V_k^{(1)}(R(t)) \cos(\omega_k t) \quad (14)$$

with $\Theta_k(t, \omega_k) \approx \omega_k t$, ω_k being the frequency of the k -th phonon mode. ΔE_k^\pm is the energy exchanged between the impinging molecule and the solid substrate due to the phonon creation and phonon annihilation processes. The energy exchanged with the phonons can be obtained directly from the transition probabilities for the excitation/deexcitation phonon processes [19].

The rotational and vibrational states of N_2 molecules, assumed as a Morse oscillator [35], were analyzed in terms of the action-angle variables using the semiclassical quantization rules [36]. Therefore, the roto-vibrational states were determined as continuous variables, as we are unable to predict some features caused by quantum effects and selection rules.

In this computational framework, we took the nitrogen molecule impinging along the normal to the surface planes starting from a distance of 10 Å and with collision energy in the range [0.04–1.2] eV. The starting distance was chosen as a compromise between reasonable calculation times for trajectory propagation and the need to consider the effects of long-range interactions. For each E_{coll} value, we propagated 30,000 trajectories, while T_S was fixed to 300 K. The initial coordinates of impinging species were randomly generated at the beginning of each trajectory, in an aiming area coinciding with the unit cell. The molecule CM impinges with polar angle $\theta = 0^\circ$, defining the selected normal approach, and azimuthal angle (ϕ) of the molecular axis was randomly chosen at the beginning of each trajectory. We can describe and follow the different elementary surface processes occurring when the N_2 molecule impinges on the surface, as the assumed PES is reactive. The impact of a molecule on a surface can give rise to scattering (elastic or inelastic), adsorption of both atoms, desorption of just one atom with the other adsorbed on the surface or desorption of both atoms as a molecule or separated.

The criteria adopted in the analysis of trajectories, leading to the assignment of a given trajectory to one of the listed reaction channels, are similar to those used in Ref. [28]. So, molecular scattering occurs if, after the interaction with the W(100) surface, the intramolecular distance (r) is lower than the distance of dissociation for the N_2 molecule and, at the same time, the distance between molecule CM and the surface is larger than 8.0 Å. On the contrary, if after the interaction with the tungsten surface the distance between N_2 CM and the surface is comparable to or smaller than the distance (≈ 5.0 Å) at which the potential approaches its asymptotic value, and r is lower than the dissociation distance, the molecule is considered trapped in the physisorption well. Further, a second “energy” criterion can be followed according to which the molecule is adsorbed when the energy available to escape from the potential well is less than the effective potential, accounting for the interaction with the surface phonons.

The trapped molecule can be subject to a steering process that can produce one of the processes listed above.

4. Conclusions

This study presents a new PES controlling the collision dynamics of N_2 molecules impinging on the W(100) surface. The long-range interaction components, defining the asymptotic behavior of the PES, have been properly characterized and represented by an ILJ function. MD simulations, performed with a semiclassical collisional model, have been exploited to characterize basic details of the collision dynamics, including its dependence on collision energy, ranging from sub-thermal up to hyper-thermal conditions. In particular,

we focused on the sticking probability, with its dependence on the collision energy; on the trapping probability, with its dependence on the surface temperature for a selected E_{coll} ; and on their comparison with the corresponding experimental determinations. This study proves that the asymptotic part of the interaction plays a crucial role in the molecular interaction dynamics since defining all relevant features of the precursor state controls the dynamics of basic phenomena occurring at the gas–surface interphase. Furthermore, the description adopted here for long-range forces is found to be more suitable than that obtained by using DFT methods with appropriate corrections.

Author Contributions: Conceptualization, methodology, formal analysis, investigation, writing—original draft preparation, writing—review and editing, M.R.; conceptualization, methodology, investigation, writing—original draft preparation, writing—review and editing, F.P. All authors have read and agreed to the published version of the manuscript.

Funding: This research received no external funding.

Data Availability Statement: The data presented in this study are available on request from the corresponding author.

Conflicts of Interest: The authors declare no conflict of interest.

References

1. Dąbrowski, A. Adsorption—from theory to practice. *Adv. Colloid Interface Sci.* **2001**, *93*, 135–224. [[CrossRef](#)]
2. Ptushinskii, Y.G. Low-temperature adsorption of gases on metal surfaces. *Low Temp. Phys.* **2004**, *30*, 1–26. [[CrossRef](#)]
3. Groß, A. *Adsorption on Surfaces in Theoretical Surface Science—A Microscopic Perspective*; Springer: Berlin/Heidelberg, Germany, 2009; pp. 101–160.
4. Hammer, B.; Norskov, J.K. Theoretical Surface Science and Catalysis—Calculations and Concepts. *Adv. Catal.* **2000**, *45*, 71–129.
5. Gao, W.; Chen, Y.; Li, B.; Liu, S.-P.; Liu, X.; Jiang, Q. Determining the adsorption energies of small molecules with the intrinsic properties of adsorbates and substrates. *Nat. Commun.* **2020**, *11*, 1196. [[CrossRef](#)]
6. Allouche, A. First principles calculations on nitrogen reactivity on tungsten surfaces. *J. Phys. Condens. Matter* **2016**, *28*, 015001. [[CrossRef](#)]
7. Penã-Torres, A.; Busnengo, H.F.; Juaristi, J.I.; Larregaray, P.; Crespos, C. Dynamics of N_2 sticking on W(100): The decisive role of van der Waals interactions. *Phys. Chem. Chem. Phys.* **2018**, *20*, 19326–19331. [[CrossRef](#)]
8. Peña-Torres, A.; Busnengo, H.F.; Juaristi, J.I.; Larregaray, P.; Crespos, C. Energy Dissipation Effects on the Adsorption Dynamics of N_2 on W(100). *J. Phys. Chem. C* **2019**, *123*, 2900–2910. [[CrossRef](#)]
9. Rettner, C.T.; Stein, H.; Schweizer, E.K. Effect of collision energy and incidence angle on the precursor-mediated dissociative chemisorption of N_2 on W(100). *J. Chem. Phys.* **1988**, *89*, 3337–3341. [[CrossRef](#)]
10. Rettner, C.T.; Schweizer, E.K.; Stein, H. Dynamics of the chemisorption of N_2 on W(100): Precursor-mediated and activated dissociation. *J. Chem. Phys.* **1990**, *93*, 1442–1454. [[CrossRef](#)]
11. Rettner, C.T.; Schweizer, E.K.; Stein, H.; Auerbach, D.J. Role of Surface Temperature in the Precursor-Mediated Dissociative Chemisorption of N_2 on W(100). *Phys. Rev. Lett.* **1988**, *61*, 986–989. [[CrossRef](#)]
12. Auerbach, D.J.; Pfnur, H.E.; Rettner, C.T.; Schlaegel, J.E.; Lee, J.; Madix, R.J. Kinetic energy and angular dependence of activated dissociative adsorption of N_2 on W(110): Observed insensitivity to incidence angle. *J. Chem. Phys.* **1984**, *81*, 2515–2516. [[CrossRef](#)]
13. Pfnur, H.E.; Rettner, C.T.; Lee, J.; Madix, R.J.; Auerbach, D.J. Dynamics of the activated dissociative chemisorption of N_2 on W(110): A molecular beam study. *J. Chem. Phys.* **1986**, *85*, 7452–7466. [[CrossRef](#)]
14. Ertl, G.; Thiele, N. XPS studies with ammonia synthesis catalysts. *Appl. Surf. Sci.* **1979**, *3*, 99–112. [[CrossRef](#)]
15. Volpillhac, G.; Salin, A. Dissociative adsorption of N_2 on the W(100) surface. *Surf. Sci.* **2004**, *556*, 129–144. [[CrossRef](#)]
16. Hafner, J.; Kresse, G. The Vienna ab-initio simulation program VASP: An efficient and versatile tool for studying the structural, dynamic and electronic properties of materials. In *Properties of Complex Inorganic Solids*; Gonis, A., Meike, A., Turchi, P.E.A., Eds.; Springer: Boston, MA, USA, 1997; pp. 69–82. [[CrossRef](#)]
17. Pirani, F.; Brizi, S.; Roncaratti, L.F.; Casavecchia, P.; Cappelletti, D.; Vecchiocattivi, F. Beyond the Lennard-Jones model: A simple and accurate potential function probed by high resolution scattering data useful for molecular dynamics simulations. *Phys. Chem. Chem. Phys.* **2008**, *10*, 5489–5503. [[CrossRef](#)] [[PubMed](#)]
18. Rutigliano, M.; Pirani, F. The role of long-range interactions on the selectivity of gaseous molecule-surface scattering. *Chem. Phys. Lett.* **2021**, *770*, 138444. [[CrossRef](#)]
19. Billing, G.D. *Dynamics of Molecule Surface Interactions*, 1st ed.; John-Wiley & Sons: New York, NY, USA, 2000; pp. 112–141.
20. Rutigliano, M.; Pirani, F. Scattering of N_2 Molecules from Silica Surfaces: Effect of Polymorph and Surface Temperature. *Molecules* **2022**, *27*, 7445. [[CrossRef](#)]
21. Rutigliano, M.; Pirani, F. Selectivity and Stereodynamics Effects in the Scattering of Nitrogen Molecules from a Graphite Surface. *J. Phys. Chem. C* **2020**, *124*, 10470–10482. [[CrossRef](#)]

22. Cambi, R.; Cappelletti, D.; Liuti, G.; Pirani, F. Generalized correlations in terms of polarizability for van der Waals interaction potential parameter calculations. *J. Chem. Phys.* **1991**, *95*, 1852–1861. [[CrossRef](#)]
23. Vidali, G.; Ihm, G.; Kim, H.-Y.; Cole, M.W. Potentials of physical adsorption. *Surf. Sci. Reports* **1991**, *12*, 133–181. [[CrossRef](#)]
24. Olney, T.N.; Cann, N.M.; Cooper, G.; Brion, C.E. Absolute scale determination for photoabsorption spectra and the calculation of molecular properties using dipole sum-rules. *Chem. Phys.* **1997**, *223*, 59–98. [[CrossRef](#)]
25. Werner, H.-J.; Meyer, W. Finite perturbation calculations for the static dipole polarizabilities of the first-row atoms. *Phys. Rev. A* **1976**, *13*, 13–16. [[CrossRef](#)]
26. Ibarguen, C.; Larregaray, P.; Peña-Torres, A.; Crespos, C. Inelastic Scattering of N₂ off W(001): Reconciling Experiment and Theory at Low Collision Energies. *J. Phys. Chem. C* **2018**, *122*, 28856–28861. [[CrossRef](#)]
27. Ibarguen Becerra, C.; Crespos, C.; Galparsoro, O.; Larregaray, P. Atomic scattering of H and N on W(100): Effect of lattice vibration and electronic excitations on the dynamics. *Surf. Sci.* **2020**, *701*, 121678. [[CrossRef](#)]
28. Rutigliano, M.; Pirani, F. Surface processes involving nitrogen molecules and atoms on silica surface at low temperature: The role of energy exchanges. *Plasma Sources Sci. Technol.* **2022**, *31*, 094006. [[CrossRef](#)]
29. Andersson, S.; Harris, J. Trapping of molecular hydrogen at surfaces via translational-rotational energy conversion. *Phys. Rev. B* **1983**, *27*, 9–14. [[CrossRef](#)]
30. Beutl, M.; Rendulic, K.D.; Castro, G.R. Does the rotational state of a molecule influence trapping in a precursor? An investigation of N₂/W(100), CO/FeSi(100) and O₂/Ni(111). *Surf. Sci.* **1997**, *385*, 97–106. [[CrossRef](#)]
31. Beutl, M.; Riedler, M.; Rendulic, K.D. Strong rotational effects in the adsorption dynamics of H₂/Pd(111): Evidence for dynamical steering. *Chem. Phys. Lett.* **1995**, *247*, 249–252. [[CrossRef](#)]
32. Kay, M.; Darling, G.R.; Holloway, S.; White, J.A.; Bird, D.M. Steering effects in non-activated adsorption. *Chem. Phys. Lett.* **1995**, *245*, 311–318. [[CrossRef](#)]
33. Gross, A.; Wilke, S.; Scheffler, M. Six-dimensional quantum dynamics of adsorption and desorption of H₂ at Pd(100) no need for a molecular precursor adsorption state. *Surf. Sci.* **1996**, *357–358*, 614–618. [[CrossRef](#)]
34. Rutigliano, M.; Cacciatore, M. Eley–Rideal recombination of hydrogen atoms on a tungsten surface. *Phys. Chem. Chem. Phys.* **2011**, *13*, 7475–7484. [[CrossRef](#)] [[PubMed](#)]
35. Huber, K.P.; Herzberg, G. Molecular Spectra and Molecular Structure: IV. In *Constants of Diatomic Molecules*; Van Nostrand Reinhold Company: New York, NY, USA, 1979; pp. 412–413.
36. Muckerman, J.T. Monte Carlo Calculations of Energy Partitioning and Isotope Effects in Reactions of Fluorine Atoms with H₂, HD, and D₂. *J. Chem. Phys.* **1971**, *54*, 1155–1164. [[CrossRef](#)]

Disclaimer/Publisher’s Note: The statements, opinions and data contained in all publications are solely those of the individual author(s) and contributor(s) and not of MDPI and/or the editor(s). MDPI and/or the editor(s) disclaim responsibility for any injury to people or property resulting from any ideas, methods, instructions or products referred to in the content.